Effect of Microstructural and Morphological Parameters on the Formability of BCC Metal Sheets

Gérald Franz, Farid Abed-Meraim, Marcel Berveiller

Effect of Microstructural and Morphological Parameters on the Formability of BCC Metal Sheets

Gérald Franz, Farid Abed-Meraim,* and Marcel Berveiller

The determination of forming limit strains in sheet metal forming industry is a useful way for quantifying metals in terms of formability. However, such forming limit diagrams (FLDs) remain very difficult to obtain experimentally. Therefore, the numerical prediction of forming limit strains represents a convenient alternative to replace this time consuming and expensive experimental process. Moreover, a combined theoretical-numerical model allows investigating the impact of essential microstructural aspects (e.g., initial and induced textures, dislocation density evolution, softening mechanisms, ...) and deformation mechanisms on the ductility of polycrystalline aggregates. In this paper, the impact of microstructural and morphological parameters, particularly the mean grain size, on the formability limit of BCC materials is investigated. To this end, an elastic–plastic self-consistent (EPSC) polycrystalline model, coupled with a bifurcation-based localization criterion, is adopted to numerically simulate FLDs. The FLDs thus determined using the bifurcation–EPSC model for an IF–Ti single-phase steel are compared to the FLDs given by ArcelorMittal, demonstrating the predictive capability of the proposed approach in investigations of sheet metal formability. The role of the averaging scheme is also shown to be significant by comparing the critical limit strains predicted with the self-consistent scale-transition scheme to those obtained with the more classical full-constraint Taylor model. Finally, numerical simulations for different values of mean grain size are provided in order to analyze the impact of mean grain size on the formability of BCC metal sheets.

1. Introduction

The concept of forming limit diagram (FLD) was first introduced by Keeler[1] and Goodwin[2] in order to display the critical limit strains leading to material failure for different strain paths, varying from uniaxial to biaxial tension conditions. The obtained curve gives a representation of the in-plane components of the limit strains, in which the major strain is plotted as a function of the minor strain in the sheet plane. This conventional tool has long been used to characterize the formability of sheet metals. Because it is now widely recognized that the onset of localized necking represents the main limitation of industrial forming processes, the FLDs are nowadays commonly determined at localization.

It should also be noted that in sheet metal forming processes several failure modes may occur (buckling, wrinkling, diffuse and localized necking), which can sometimes be coupled with damage phenomena. A unified approach considering all these mechanisms remains very difficult to achieve and hence the present work only focuses on the onset of strain localization due to macroscopic shear band formation.

Because experimental FLD measurements are a complex task and notably because of the strong influence of several physical factors, such as microstructural and textural anisotropy, various theoretical models have been developed to predict localized necking. These are mainly based either on imperfection theories, in particular the Marciniak–Kuczynski (M–K) model[3] and its generalization by Hutchinson and Neale,[4] or on bifurcation analysis, such as Rice's localization model.[5,6] Note that the M–K approach is widely adopted to simulate FLDs, due to its flexibility and simple use for industrial applications; however, the main drawback of this theory is the high sensitivity of the results to some parameters such as the initial thickness defect or the critical value of the threshold

[*] G. Franz
LTI[Q1]EA 3899–IUT Amiens, Avenue des Facultés – Le Bailly, 80025 Amiens, Cedex 1, France
F. Abed-Meraim, M. Berveiller
LEM3, UMR CNRS 7239–Arts et Métiers ParisTech, 4 rue Augustin Fresnel 57078 Metz, Cedex 3, France
Email: farid.abed-meraim@ensam.eu
F. Abed-Meraim
DAMAS[Q2]Laboratory of Excellence on Design of Alloy Metals for low-mAss Structures, Université de Lorraine, France

at which localization is said to occur. For these reasons, the bifurcation approach has been preferred in the current study, because it does not require any additional adjusting parameter and can be used within a fully three-dimensional framework. This bifurcation analysis is based on the formation of strain localization bands corresponding to jumps of some mechanical fields across discontinuity interfaces.

The main objective of the current paper is to investigate the impact of microstructural and morphological parameters on formability limits of BCC materials, which can provide guidelines for the design of new materials with enhanced ductility properties. For this purpose, the bifurcation approach will be coupled with an elastic–plastic self-consistent (EPSC) polycrystalline formulation.

The ability of the present multiscale model to accurately predict the macroscopic behavior of single-phase polycrystalline steels during monotonic and sequential loading paths has been shown in Franz et al.[7,8]

First, the EPSC multiscale model and the bifurcation theory are presented in Section 2. Then, the main results obtained with the present model are presented in Section 3 in terms of strain localization analyses for a ferritic single-phase steel, where the impact of mean grain size is investigated for a 1000-grain polycrystalline aggregate similar to the ferritic single-phase steel IF–Ti. Finally, some concluding remarks are drawn in Section 4.

2. Theoretical Framework

2.1. Local Elastic–Plastic Constitutive Modeling

A detailed presentation of the EPSC multiscale model can be found in Franz et al.[7,8] Only the main equations are outlined here.

Three different essential mechanisms – twinning, phase transformation and crystallographic slip – generally result in irreversible deformation. The present model only focuses on the crystallographic slip mechanism, and the corresponding deformation of BCC metals will thus be considered. For this type of materials, 24 independent slip systems will be assumed potentially active, i.e., the slip planes {110} and {112} and the slip directions $\langle 111 \rangle$.

The elastic distortion of the lattice and the plastic flow due to slip on the crystallographic planes can be considered as the most important aspects of single crystal behavior. The adopted formulation is based on pioneering contributions.[9–15] The single crystal elastic–plastic constitutive law is written within the large strain framework and is defined through the derivation of a tangent modulus $\mathbf{l}$ relating the nominal stress rate $\dot{\mathbf{n}}$ to the velocity gradient $\mathbf{g}$:

$$\dot{\mathbf{n}} = \mathbf{l} : \mathbf{g} \tag{1}$$

An additive decomposition of the velocity gradient $\mathbf{g}$ is commonly used:

$$\mathbf{g} = \mathbf{d} + \mathbf{w} \tag{2}$$

where the symmetric part $\mathbf{d}$ designates the total strain rate and the anti-symmetric part $\mathbf{w}$ corresponds to the total rotation rate.

These two parts can additionally be split into a plastic and an elastic part as:

$$\mathbf{d} = \mathbf{d}^{\mathrm{e}} + \mathbf{d}^{\mathrm{p}}, \quad \mathbf{w} = \mathbf{w}^{\mathrm{e}} + \mathbf{w}^{\mathrm{p}} \tag{3}$$

The plastic part of the velocity gradient is related to the slip rates $\dot{\gamma}^g$ by:

$$\mathbf{g}^{\mathrm{p}} = \mathbf{d}^{\mathrm{p}} + \mathbf{w}^{\mathrm{p}} = \sum\nolimits_g \dot{\gamma}^g \vec{m}^{\,g} \otimes \vec{n}^{\,g} \tag{4}$$

where $\vec{m}^{\,g}$ is the vector parallel to the slip direction of the slip plane g with normal $\vec{n}^{\,g}$, $\dot{\gamma}^g$ is the associated slip rate.

From Equation (4), the plastic strain rate $\mathbf{d}^{\mathrm{p}}$ and plastic spin $\mathbf{w}^{\mathrm{p}}$ can easily be written in terms of the Schmid tensors $\mathbf{R}^g$ and $\mathbf{S}^g$, defined as the symmetric and anti-symmetric parts, respectively, of the tensor product $\vec{m}^{\,g} \otimes \vec{n}^{\,g}$.

It is necessary to know the slip rates of active slip systems in order to determine the expression of the local tangent modulus $\mathbf{l}$. The adopted procedure for the active slip system selection will be briefly described here; more details on this method and its validation can be found in Franz et al.[7]

For plastic behavior, the plastic flow rule for a given slip system g is commonly expressed by distinguishing the effectively active slip systems from those potentially active, leading to the existence of several possible subsets of active systems:

$$\begin{cases} \tau^g < \tau_c^g \Rightarrow \dot{\gamma}^g = 0 \\ \tau^g = \tau_c^g \text{ and } \dot{\tau}^g \leq 0 \Rightarrow \dot{\gamma}^g = 0 \\ \tau^g = \tau_c^g \text{ and } \dot{\tau}^g > 0 \Rightarrow \dot{\gamma}^g \geq 0 \end{cases} \tag{5}$$

where the resolved shear stress acting on a given slip system g is given by:

$$\tau^g = \boldsymbol{\sigma} : \mathbf{R}^g \tag{6}$$

and its evolution can be expressed using the co-rotational derivative of the Cauchy stress tensor $\boldsymbol{\sigma}^{\nabla}$:

$$\dot{\tau}^g = \boldsymbol{\sigma}^{\nabla} : \mathbf{R}^g \tag{7}$$

In order to select the active slip systems and derive their slip rates within an elastic–plastic modeling framework, a

new approach, inspired by viscoplastic formulations, allows replacing relation (5) with a rate-independent regularization technique $\dot{\gamma}^g = k^g\left(\tau^g, \tau_c^g, \dot{\tau}^g\right)\dot{\tau}^g$

Finally, combining the previous relations with the single crystal elastic–plastic law given by Equation (1), the expression of the tangent modulus $\mathbf{l}$ is given in indicial notation by:

$$\begin{aligned} l_{ijkl} = {} & C_{ijkl} - \frac{1}{2}\left(\sigma_{ik}\delta_{jl} - \sigma_{il}\delta_{jk}\right) - \frac{1}{2}\left(\delta_{ik}\sigma_{jl} + \delta_{il}\sigma_{jk}\right) \\ & - \sum\nolimits_{g,h}\left(C_{ijmn}R^g_{mn} + S^g_{im}\sigma_{mj} - \sigma_{im}S^g_{mj}\right)M^{gh} \\ & \times \left(R^h_{pq}C_{pqkl} - R^h_{pq}\sigma_{pq}\delta_{kl}\right) \end{aligned} \tag{8}$$

It can be observed that this local tangent modulus exhibits elastic and plastic parts, which contain several additional terms due to the large strain framework.

In the present model, it is assumed that the single crystal hardening law is given by the expression of the evolution of critical resolved shear stress rate $\dot{\tau}_c$ with slip rate $\dot{\gamma}$ for the whole system:

$$\dot{\tau}_c^g = \sum\nolimits_{h=1}^{n_{gl}} H^{gh}\dot{\gamma}^h \tag{9}$$

in which summation is over the active slip systems, whose number is n_{gl}, and where H^{gh} is the hardening interaction matrix defining self-hardening and latent hardening.

Hardening is mainly due to mobile dislocation interactions with lattice and pinned obstacles. During plastic strain, dislocations are first created, stored and then annihilated when their densities become sufficiently large. Kocks[16] first proposed a law describing the evolution of the dislocation densities without a specified annihilation mechanism. This law has been improved later by Essmann and Mughrabi[17] considering the annihilation of close dislocations:

$$\dot{\rho}^g = \frac{1}{b}\left(\frac{1}{L^g} - 2y_c\rho^g\right)\dot{\gamma}^g \tag{10}$$

where b is the magnitude of the Burgers vector, L^g is the mean free path of dislocations on the slip system g, and y_c is the critical annihilation distance of dislocations.

The mean free path can be related to the mean grain size D and expressed thanks to a parameter g_0 specific to the dislocation storage:

$$\frac{1}{L^g} = \frac{1}{D} + \frac{\sqrt{\sum_{h=1,h\neq g}^{n_{gl}}\rho^h}}{g_0} \tag{11}$$

The relationship between critical resolved shear stress and dislocation densities has been extended to the multislip case[18] as:

$$\tau_c^g = \tau_0^g + \alpha\mu b\sqrt{\sum_{h=1}^{n_{gl}} a^{gh}\rho^h} \tag{12}$$

where τ_0^g is the initial critical resolved shear stress, α is a constant related to the stability of the dislocation configurations, μ is the shear modulus, a^{gh} is the anisotropy interaction matrix, and ρ^h is the mean dislocation density for slip system h. The anisotropy interaction matrix introduced by Franciosi[18] and expanded by Hoc[19] will be used, in which the different components are defined by nine parameters depending on the nature of the dislocation interactions (e.g., coplanar or collinear systems…).

Differentiating Equation (12) and using Equation (9) and (10), the hardening matrix is expressed as:

$$H^{gh} = \frac{\alpha\mu}{2\sqrt{\sum_{k=1}^{n_{gl}} a^{gk}\rho^k}}\, a^{gh}\left(\frac{1}{L^h} - 2y_c\rho^h\right) \tag{13}$$

2.2. One-Site Self-Consistent Approximation

In order to simulate the overall macroscopic response of polycrystalline aggregates, thanks to knowledge of the behavior of their individual constituents, a self-consistent scheme is employed. A detailed presentation of this averaging approach is given by Lipinski and Berveiller,[14] Lipinski et al.[15] and Franz et al.[7] Only the main equations are outlined hereafter.

The incremental form of the single crystal constitutive law given by Equation (1) can still be used to express the macroscopic behavior law, making use of the macroscopic tangent modulus $\mathbf{L}$, such as:

$$\dot{\mathbf{N}} = \mathbf{L} : \mathbf{G} \tag{14}$$

The overall nominal stress rate $\dot{\mathbf{N}}$ and the overall velocity gradient $\mathbf{G}$ for the aggregate are defined as the volume averages of their local counterparts $\dot{\mathbf{n}}$ and $\mathbf{g}$, respectively:

$$\begin{cases} \mathbf{G} = \dfrac{1}{V}\displaystyle\int_V \mathbf{g}(\mathbf{x})\, dv = \overline{\mathbf{g}(\mathbf{x})} \\ \dot{\mathbf{N}} = \dfrac{1}{V}\displaystyle\int_V \dot{\mathbf{n}}(\mathbf{x})\, dv = \overline{\dot{\mathbf{n}}(\mathbf{x})} \end{cases} \tag{15}$$

In order to solve the averaging problem, the following fourth-order concentration tensor is commonly introduced:

$$\mathbf{g}(\mathbf{x}) = \mathbf{A}(\mathbf{x}) : \mathbf{G} \tag{16}$$

A systematic expression for the macroscopic tangent modulus is easily obtained by combining the local behavior law, Equation (1), with Equation (14)–(16):

$$\mathbf{L} = \frac{1}{V}\int_V \mathbf{l}(\mathbf{x}) : \mathbf{A}(\mathbf{x})\, dv = \overline{\mathbf{l}(\mathbf{x}) : \mathbf{A}(\mathbf{x})} \tag{17}$$

It is also assumed that the polycrystalline aggregate is composed of ellipsoidal grains with different crystallographic orientations and that for each individual grain I, the behavior and mechanical fields are homogeneous. The expression of the concentration tensor $\mathbf{A}^I$ related to grain I can then be written as:

$$\mathbf{A}^I = \left(\mathbf{I} - \mathbf{T}^{II} : \left(\mathbf{l}^I - \mathbf{L}\right)\right)^{-1} : \overline{\left(\mathbf{I} - \mathbf{T}^{II} : \left(\mathbf{l}^I - \mathbf{L}\right)\right)^{-1}}^{-1} \tag{18}$$

where $\mathbf{T}^{II}$ denotes the interaction tensor for grain I, which is related to Eshelby's tensor[20] for an ellipsoidal inhomogeneity. For a polycrystalline aggregate comprising Ng grains with a respective volume fraction f^I, the one-site self-consistent expression corresponding to the self-consistent scheme in the sense of Hill[21] can be finally obtained as:

$$\mathbf{L} = \sum_{I=1}^{Ng} f^I \mathbf{l}^I : \mathbf{A}^I \tag{19}$$

Note that the classical full-constraint Taylor model can be derived as a special case of the self-consistent scheme by considering that the deformation within each grain is equal to the macroscopic deformation. This amounts to taking the fourth-order concentration tensor $\mathbf{A}$ equal to the fourth-order identity tensor, which leads to an effective modulus simply given by:

$$\mathbf{L} = \frac{1}{V}\int_V \mathbf{l}(\mathbf{x})dv = \overline{\mathbf{l}(\mathbf{x})} \tag{20}$$

A last point concerns the integration within the model of the morphological and crystallographic evolutions for each grain during loading. The crystallographic and morphological orientation of each grain is denoted respectively by the Euler angles φ_1, ϕ, φ_2 and φ'_1, ϕ', φ'_2, according to Bunge's notation.[22,23] A schematic representation defining these three Euler's angles is given in **Figure 1**. For the morphological orientation, these angles define the orientation of the principal coordinate system of the ellipsoid representing the grain relative to the coordinate system (RD, TD, ND) of the sample.

The change of crystallographic orientation is due to elastic rotation rate $\mathbf{w}^e$.[13,24] The evolution of Euler's angles with the lattice rotation is governed by the following equations:

$$\begin{cases} \dot{\varphi}_1 = -w^e_{12} + \dfrac{\cos\phi}{\sin\phi}\left(w^e_{13}\cos\varphi_1 + w^e_{23}\sin\varphi_1\right) \\ \dot{\phi} = -w^e_{23}\cos\varphi_1 + w^e_{13}\sin\varphi_1 \\ \dot{\varphi}_2 = -\dfrac{1}{\sin\phi}\left(w^e_{13}\cos\varphi_1 + w^e_{23}\sin\varphi_1\right) \end{cases} \tag{21}$$

With regard to the morphology of the grain, the morphological orientation evolves with the total rotation rate as:

$$\begin{cases} \dot{\varphi}'_1 = -w_{12} + \dfrac{\cos\phi'}{\sin\phi'}\left(w_{13}\cos\varphi'_1 + w_{23}\sin\varphi'_1\right) \\ \dot{\phi}' = -w_{23}\cos\varphi'_1 + w_{13}\sin\varphi'_1 \\ \dot{\varphi}'_2 = -\dfrac{1}{\sin\phi'}\left(w_{13}\cos\varphi'_1 + w_{23}\sin\varphi'_1\right) \end{cases} \tag{22}$$

The shape of the grains is taken as an ellipsoid, which is represented by its half-axes a, b and c. The morphological

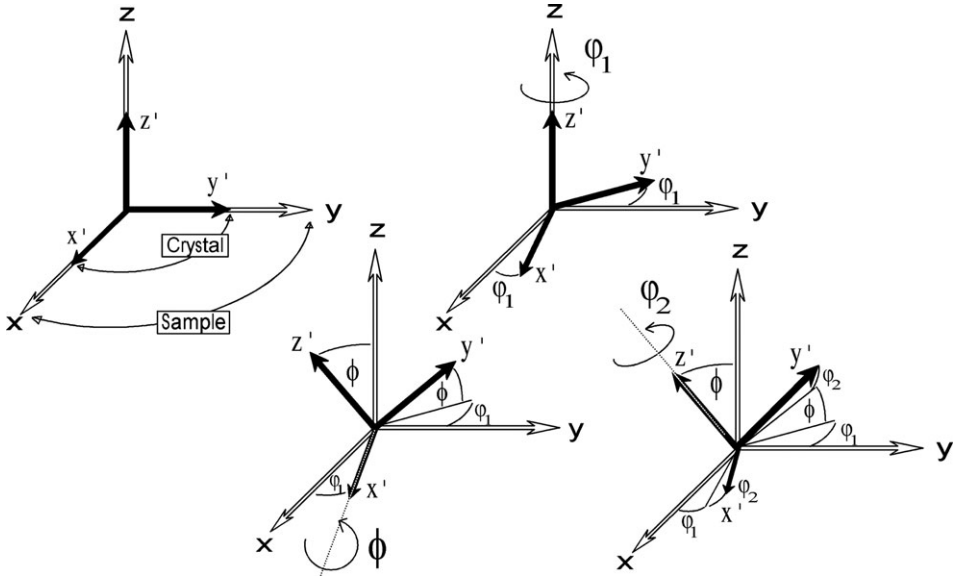

Figure 1. Schematic representation defining the three Euler angles φ_1, ϕ, φ_2 according to Bunge's notation.

evolution is due to the total deformation rate as:

$$\begin{cases} \dot{a} = a\, g_{11}^{ell} \\ \dot{b} = b\, g_{22}^{ell} \\ \dot{c} = c\, g_{33}^{ell} \end{cases} \quad (23)$$

where $\mathbf{g}^{ell}$ is the projection of the velocity gradient onto the morphological frame.

2.3. Localization Bifurcation Criterion

The so-called Rice's localization criterion[5,6] corresponds to a bifurcation of the governing equations, which is associated with admissible jumps for strain and stress rates across a shear band as illustrated in **Figure 2**.

Because field equations have to be satisfied, the kinematic condition for the strain rate jump is:

$$[\mathbf{G}] = \mathbf{G}^{+} - \mathbf{G}^{-} = \boldsymbol{\kappa} \otimes \boldsymbol{\upsilon} \quad (24)$$

where $\boldsymbol{\kappa}$ denotes the jump amplitude and $\boldsymbol{\upsilon}$ is the unit normal to the shear band.

On the other hand, the continuity of the stress rate vector has to be verified for the forces along the interface created by the localization band:

$$\left[\dot{\mathbf{N}}^{T}\right] \cdot \boldsymbol{\upsilon} = \mathbf{0} \quad (25)$$

At the incipience of bifurcation, it is commonly considered that the tangent modulus is the same on each part of the band. By using the constitutive law (14) along with Equation (24) and (25), the following condition is derived:

$$(\boldsymbol{\upsilon} \cdot \mathbf{L} \cdot \boldsymbol{\upsilon}) \cdot \boldsymbol{\kappa} = \mathbf{0} \quad (26)$$

A non-trivial solution for the linear system of Equation (26), , corresponding to the occurrence of bifurcation and thus to the existence of at least one non-zero $\boldsymbol{\kappa}$, is obtained when the following condition is satisfied:

$$det(\boldsymbol{\upsilon} \cdot \mathbf{L} \cdot \boldsymbol{\upsilon}) = 0 \quad (27)$$

The associated normal $\boldsymbol{\upsilon}$, in the three-dimensional space, defines the localization band orientation, while the amplitude of the jump cannot be calculated directly.

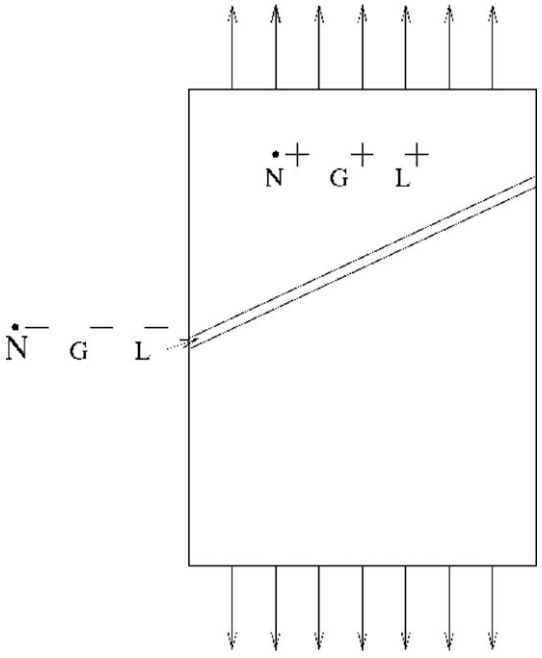

Figure 2. Localization of the deformation along a shear band.

3. Numerical Results – Prediction of Ductility Limits for BCC Materials

3.1. Material Parameter Identification and Validation

The following results are obtained for a ferritic single-phase steel, denoted IF–Ti, for which the identified material parameters are reported in **Table 1**. An initially random texture defined by 1000 crystallographic orientations is considered.

It is necessary to identify four parameters relative to the single crystal modeling. The three first parameters: initial critical resolved shear stress τ_0^g, parameter g_0, which is related to the mean free path of dislocations, and critical annihilation distance of dislocations y_c are determined using only two mechanical tests, i.e., a uniaxial tensile test (or a simple shear test) and a reverse shear test. The mean grain size D can be easily identified using optical micrography.

The model is then validated by comparison with experimental stress–strain responses corresponding to various mechanical tests (uniaxial tensile test, simple shear test, plane strain tensile test, biaxial tensile test, balanced biaxial tensile test, Bauschinger test, orthogonal test) at different orientations with respect to the rolling direction. As depicted in **Figure 3**, modeling results are in agreement with the experimental ones for the IF–Ti steel.

Parameters	τ_{c0} [110]	τ_{c0} [112]	g_0	y_c	D
Values	55 MPa	55 MPa	90	3.25 nm	20 μm

Table 1. Material parameters used for the IF–Ti single-phase steel.

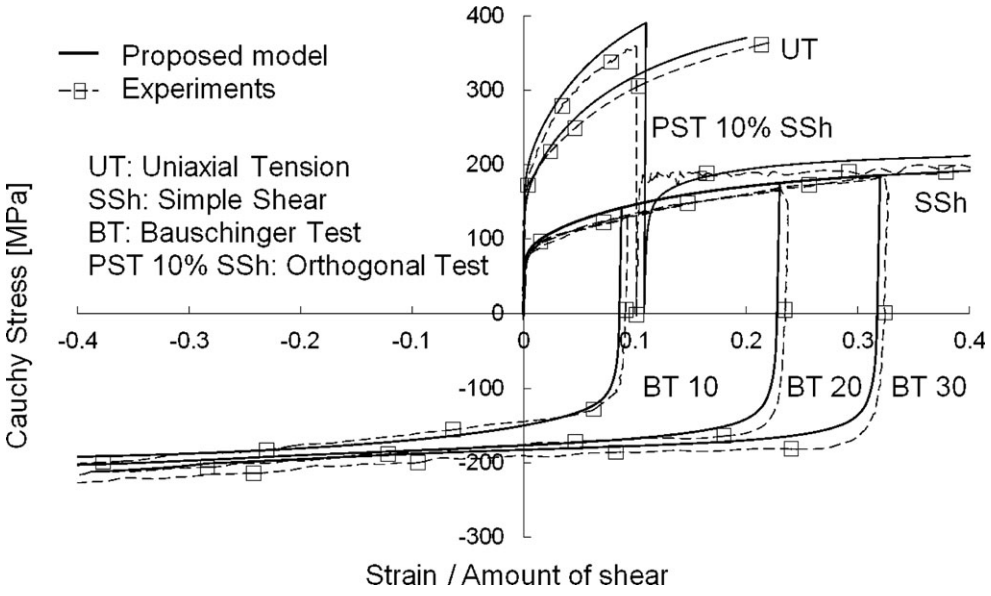

Figure 3. Comparison between the proposed model and the experiments for the studied IF–Ti single-phase steel for different linear and sequential loading paths performed perpendicular to the rolling direction (PST 10% SSh refers to a cross test consisting of 10% plane strain tension followed by simple shear, while BT refers to reverse shear tests at 10%, 20%, and 30% of shear prestrain).

3.2. Comparison with Reference Model

In this Section, the Bifurcation–EPSC approach is applied to the IF–Ti steel for FLD prediction and the obtained diagram is compared to the FLD provided by ArcelorMittal, as reported in **Figure 4**. The ArcelorMittal FLD model[25,26] can be considered as reference for comparison because it has proven its reliability in predicting formability for linear strain paths for a wide range of grades of sheet metals, for which experimental FLDs have been simultaneously measured and compared.

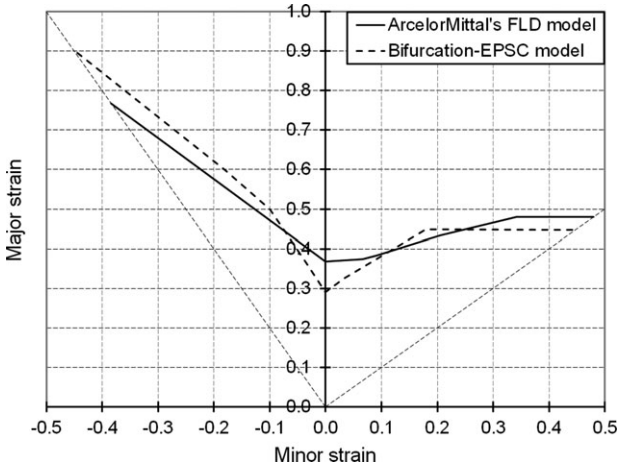

Figure 4. Simulated FLDs associated with linear strain paths for the IF–Ti single-phase steel obtained with bifurcation–EPSC and ArcelorMittal's models.

As shown in Figure 4, the FLD obtained with the Bifurcation–EPSC model for the studied ferritic single-phase steel is close to the ArcelorMittal FLD. Having assessed the predictive capability of the present model in the determination of forming limit strains, attention will be directed now towards the investigation of the impact of microstructural parameters on formability limits of BCC materials.

3.3. Simulation of the Strain Paths

The FLD depicts the limit strain values determined for different strain paths, covering uniaxial tension, through plane strain tension, to equibiaxial tension. Different ways are possible to define these strain paths, which correspond to different choices for the applied loading or prescribed boundary conditions. We propose here to investigate the impact of such choices on the determination of FLDs for the previously studied IF–Ti steel. The same set of parameters, as reported in Table 1, is used for these simulations.

In this Section, the different strain paths can be obtained by prescribing a complementary set of components for two parameterization tensors, in order to set the associated boundary value problem. The first choice consists of prescribing all strain-rate tensor components as follows:

$$\mathbf{d} = \mathrm{d}_{11}\begin{bmatrix} 1 & 0 & 0 \\ 0 & \rho & 0 \\ 0 & 0 & -1-\rho \end{bmatrix} \tag{28}$$

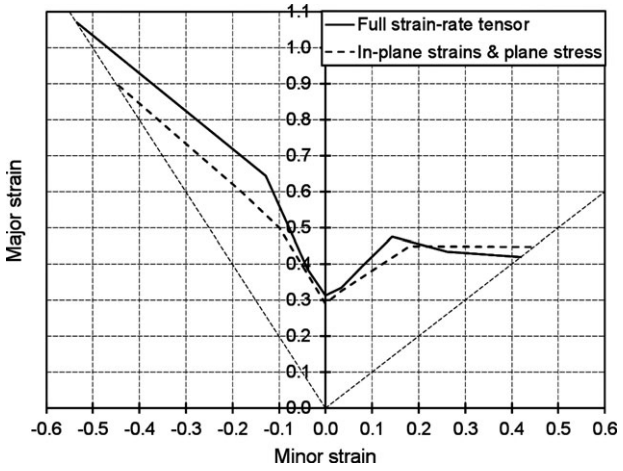

Figure 5. Simulated FLDs associated with linear loading paths for the IF–Ti single-phase steel obtained with the bifurcation–EPSC model: two different ways to prescribe the strain paths.

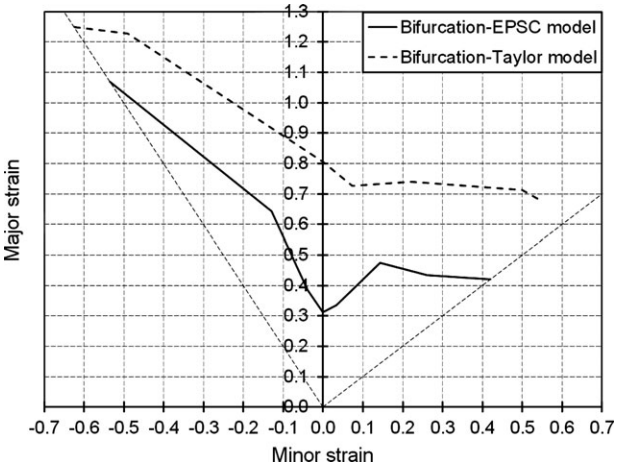

Figure 6. Simulated FLDs associated with linear loading paths for the IF–Ti single-phase steel as obtained with bifurcation–EPSC and bifurcation–Taylor models.

and the strain paths are defined by varying the in-plane strain ratio ρ between -0.5 (uniaxial tensile test) and 1 (equibiaxial tensile test).

Another way to simulate the strain paths is by prescribing the in-plane strain components, with the same definition for the in-plane strain ratio ρ, in conjunction with the plane-stress conditions.

Figure 5 shows the limit strains as predicted by the two parameterization procedures. One can observe that the formability limits predicted with the second procedure (i.e., by imposing the in-plane strain components along with plane-stress conditions) are lower, in the whole, than those obtained with the first procedure (i.e., full strain components as given by Equation (28)). This trend is in general agreement with the fact that plane-stress conditions tend to precipitate strain localization (i.e., the consideration of the through-thickness stresses has been shown to delay the critical limit strains).

3.4. Influence of the Scale-Transition Scheme

The influence of the averaging scheme on the predicted limit strains is investigated in this Section. Numerical FLDs obtained with two different scale-transition schemes (i.e., the self-consistent model (bifurcation–EPSC model) and Taylor's model (bifurcation–Taylor model)) for the studied IF–Ti steel are reported in **Figure 6** and compared.

One can observe that, for the whole range of loading paths, the limit strains predicted with the full-constraint Taylor model are found to be particularly overestimated in comparison with those predicted with the self-consistent model. The impact of the adopted homogenization rule on formability limit prediction for BCC and FCC materials has been recently investigated using rate-sensitive crystal plasticity models in conjunction with the M–K approach.[27,28] These works have shown that, in the biaxial-stretching domain, the full-constraint Taylor model predicts higher limit strains than those obtained with the self-consistent scheme for BCC materials.

3.5. Effect of Mean Grain Size

Figure 7 illustrates the effect of the mean grain size on the ductility limit of the studied IF–Ti steel. In this investigation, all the parameters in Table 1 are held constant except the mean grain size D. It is known that a decrease in the mean grain size produces higher-strength materials but, in

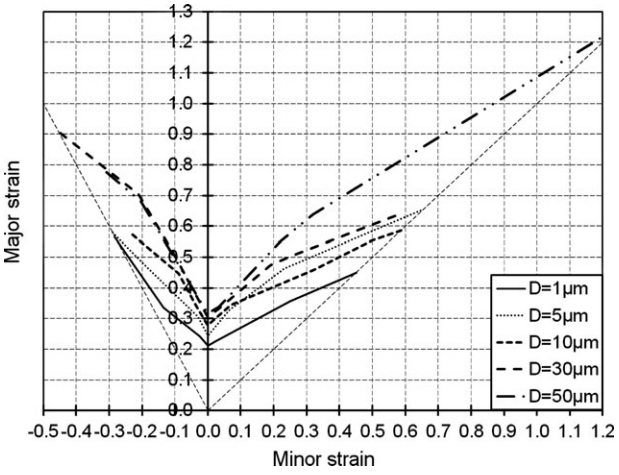

Figure 7. Simulated FLDs associated with linear loading paths for the IF–Ti single-phase steel as obtained with the bifurcation–EPSC model: Effect of the mean grain size.

turn, induces a drop in ductility. This experimental observation is well reproduced by the proposed model, and the results shown in Figure 7 are in general agreement with the above statement.

4. Conclusions

In this paper, an elastic–plastic self-consistent (EPSC) polycrystalline model has been combined with Rice's localization criterion to investigate the influence of microstructural and morphological parameters on the formability of BCC materials in sheet forming processes. Numerical FLDs have been determined for ferritic single-phase steel, denoted IF–Ti, and compared to reference FLDs provided by ArcelorMittal. To this end, the macroscopic behavior law has been first accurately modeled in order to take into account the most important softening mechanisms. It has been shown that the EPSC multiscale model correctly reproduces the stress–strain responses for various mechanical tests (linear and non-linear loading paths). The adopted bifurcation-based ductility criterion allows the prediction of FLDs, which are found to be close to reference FLDs. It has also been shown that the self-consistent scheme predicts more realistic forming limit strains than the full-constraint Taylor model does.

Finally, the influence of the mean grain size on formability has been investigated and the model predictions led to higher limit strains for larger mean grain size values, in agreement with experimental observations.

The proposed theoretical and numerical tool allows ductility prediction of new materials at the very early stage of the design of new grades of steel and thus provides a useful tool for steelmakers. Its main interest is to allow comparisons in terms of formability for various materials and to reveal the impact of microstructural effects on ductility. Therefore, it can be advantageously used to optimize the ductility of new steels or to design materials with desired formability.

Acknowledgements

Part of this research has been performed within a project jointly funded by ArcelorMittal and CNRS. The first author is grateful to ArcelorMittal Research and CNRS for the financial support of his PhD.

Received: April 29, 2013

Keywords: forming limit diagrams; crystal plasticity; self-consistent scale transition; bifurcation criterion; BCC materials

References

[1] S. P. Keeler, *Sheet Metal Indust.* **1965**, *42*, 683.
[2] G. M. Goodwin, SAE Paper No. 680093 **1968**.
[3] Z. Marciniak, K. Kuczynski, *Int. J. Mech. Sci.* **1967**, *9*, 609.
[4] J. W. Hutchinson, K. W. Neale, in *Mechanics of Sheet Metal Forming*, (Eds: D. P. Koistinen, N. M. Wang), Plenum Press, New York, **1978**, pp. 127–153.
[5] J. W. Rudnicki, J. R. Rice, *J. Mech. Phys. Solids* **1975**, *23*, 371.
[6] J. R. Rice, In: 14th International Congress of Theoretical and Applied Mechanics, **1976**, 207.
[7] G. Franz, F. Abed-Meraim, J. P. Lorrain, T. Ben Zineb, X. Lemoine, M. Berveiller, *Int. J. Plasticity* **2009**, *25*, 205.
[8] G. Franz, F. Abed-Meraim, M. Berveiller, Int. J. Plasticity **2013**, http://dx.doi.org/10.1016/j.ijplas.2013.02.001
[9] R. Hill, *J. Mech. Phys. Solids* **1966**, *14*, 95.
[10] R. J. Asaro, *Acta Metall.* **1979**, *27*, 445.
[11] R. J. Asaro, *J. Appl. Mech.* **1983**, *50*, 921.
[12] S. Nemat-Nasser, M. M. Mehrabadi, T. Iwakuma, In: *Three-dimensional constitutive relations and ductile fracture*, (Ed: S Nemat-Nasser), North-Holland, Amsterdam **1981**, 157.
[13] T. Iwakuma, S. Nemat-Nasser, *Proc. R. Soc. Lond. A* **1984**, *394*, 87.
[14] P. Lipinski, M. Berveiller, *Int. J. Plasticity* **1989**, *5*, 149.
[15] P. Lipinski, M. Berveiller, E. Reubrez, J. Morreale, *Arch. Appl. Mech.* **1995**, *65*, 291.
[16] U. F. Kocks, *J. Eng. Mat. Tech.* **1976**, *98*, 76.
[17] U. Essmann, H. Mughrabi, *Philos. Mag. A* **1979**, *40*, 731.
[18] P. Franciosi, PhD Thesis, Paris North University, France, **1984**.
[19] T. Hoc, PhD Thesis, Ecole Centrale de Paris, France, **1999**.
[20] J. Eshelby, *Proc. R. Soc. Lond. A* **1957**, *241*, 376.
[21] R. Hill, *J. Mech. Phys. Solids* **1965**, *13*, 89.
[22] H. J. Bunge, In: *Mathematische Methoden der Texturanalyse*, Akademie-Verlag, Berlin **1969**.
[23] H. J. Bunge, In: *Texture Analysis in Materials Science*[Q3], Butterworths, London **1982**.
[24] E. V. Nesterova, B. Bacroix, C. Teodosiu, *Met. Mat. Trans. A* **2001**, *32A*, 2527.
[25] F. Cayssials, In: 20th IDDRG Conference. Brussels **1998**.
[26] F. Cayssials, X. Lemoine, In: 24th IDDRG Conference. Besançon **2005**.
[27] J. W. Signorelli, M. A. Bertinetti, P. A. Turner, *Int. J. Plasticity* **2009**, *25*, 1.
[28] J. W. Signorelli, M. J. Serenelli, M. A. Bertinetti, *J. Mat. Proc. Tech.* **2012**, *212*, 1367.